3D-printable low-reduction cycloidal gearing for robotics

Conference Paper · October 2022

DOI: 10.1109/IROS47612.2022.9982006

2 authors, including:

Wesley Roozing
University of Twente
34 PUBLICATIONS **496** CITATIONS

3D-printable low-reduction cycloidal gearing for robotics

Wesley Roozing[1] and Glenn Roozing[2]

***Abstract*— The recent trend towards low reduction gearing in robotic actuation has revitalised the need for high-performance gearing concepts. In this work we propose compact low-reduction cycloidal gearing, that is 3D-printable and combined with off-the-shelf components. This approach presents an enormous potential for high performance-to-cost implementations. After discussing parameter selection and design considerations, we present a prototype that is combined with a low-cost brushless motor to demonstrate its potential. Extensive experimental results demonstrate high performance, including >40 Nm torque, low friction and play, and high impact robustness. The results show that the proposed approach can yield viable gearbox designs.**

I. Introduction

In the last two to three decades, robots have typically employed high-ratio gearing to achieve sufficient output torque from their electric motors. Typically, high-performance implementations have utilised harmonic drives, for their compactness, precision, high gear ratios, and low backlash.

However, the recent trend towards lower gear ratios, i.e. quasi-direct-drive actuators [1]–[8], has revitalised the need for high-performance gearing. Low reduction ratios are difficult to realise with harmonic drives, and they are very inefficient at low speeds and torques [9]. As a result, planetary, wolfrom, cycloidal, and other types of gearing have gained in popularity [10]–[12]. Although (compound) planetary gears and their variants have received significantly more attention, their (shock) robustness, torque capacity, and backlash properties are limited. Cycloidal drives present excellent properties for modern robots, including high (shock/impact) robustness, torsional stiffness, torque capacity, and efficiency [13]–[15]. Many of these properties are owed to the significantly larger force transmission area, absence of shear stress, and rolling contacts [13], [16].

Over the years many authors have analysed different aspects of cycloidal drive gearing to optimise its design [16]–[19], including tooth profile modifications to account for machining and other tolerances [20], [21]. In particular, it has been found that efficiency can be greatly increased by using (needle) bearings instead of bushings or 'free' rollers [9], [15], [22]. This increases peak efficiency to the level of planetary gears of approximately 90%. However, it should be noted that with certain modifications, so-called 'non-pinwheel' designs can achieve similar efficiencies [23].

Recently several compact cycloidal drives aimed at robotics have been proposed [15], [24]. The high-performance biped Cassie has also been reported to utilise cycloidal drives [25], citing their robustness and efficiency as primary benefits, but no further details are available.

Fig. 1: Cycloidal drive prototype with motor and gearbox separated.

An additional benefit of cycloidal drives, so far unexplored in robotics literature, is that they are ideally suited to be 3D printed, while remaining robust as a result of their large contact area for power transmission and absence of shear stress. This allows for implementations with very high performance/cost ratio, as will be shown in this paper. We have developed a compact low-reduction cycloidal drive gearbox, that is low-cost, 3D-printable, and uses off-the-shelf bearings and steel components.

The contributions of this paper are as follows:

- A parameter selection procedure to guide the design of cycloidal gearing designs that can be 3D printed and are low cost (€ 98 incl. output bearing);
- An open-source design of a 11:1 cycloidal gearbox that combined with a low-cost brushless motor can achieve >40 Nm output torque and 53 rad/s peak output speed;
- Extensive experimental results that validate the performance characteristics of the prototype and show the approach can yield viable gearing designs.

The remainder of this paper is outlined as follows. Sec. II provides a brief overview of the working principle and main geometry of cycloidal drives. Sec. III discusses design considerations and parameter selection, followed by the the proposed design and realised prototype in Sec. IV. Experimental validation is presented in Sec. V, followed by a discussion in Sec. VI. Finally, Sec. VII concludes the paper.

[1]W. Roozing is with the Robotics & Mechatronics (RaM) group, University of Twente, The Netherlands. E-mail: w.roozing at utwente.nl.

[2]G. Roozing is with Auto Elect B.V., The Netherlands. E-mail: glenn.roozing at auto-elect.nl.

II. Working principle and geometry

The basic working principle of a cycloidal drive is that of a disk rolling about an outer ring of larger radius. As it rolls, the disk rotates at a velocity that is proportional to the relative radii, which provides the gearing ratio of the gearbox. Teeth and rollers are then added to provide mechanical positive fit for higher power transfer. The rolling of the disk is driven by the input shaft, with an eccentric cam that keeps the disk in contact with the rollers. The rotating motion of the disk is transmitted to the output shaft via output holes in the cycloid disk and pins located on the output disk. We refer to the video attachment for an intuitive animation of the principle.

The basic geometry is shown in Fig. 2. The cycloidal disk (shown in blue), rolls over N_r (here 12) rollers (in black) on the outside perimeter at radius R, each with radius R_r. It is driven by the eccentric cam, with radius R_e, on the input shaft (in green), which rotates about the input shaft rotation axis with an eccentricity E. To transfer the cycloid disk motion to the output shaft, there are N_o (here 6) output holes and corresponding pins. The holes are located at a radius L_o on the disk, with radius R_oh. The output pins (shown in red) have a radius R_o. Lastly, we denote the input–output and minimum output–edge thickness in the cycloid disk as L_io and L_or, respectively.

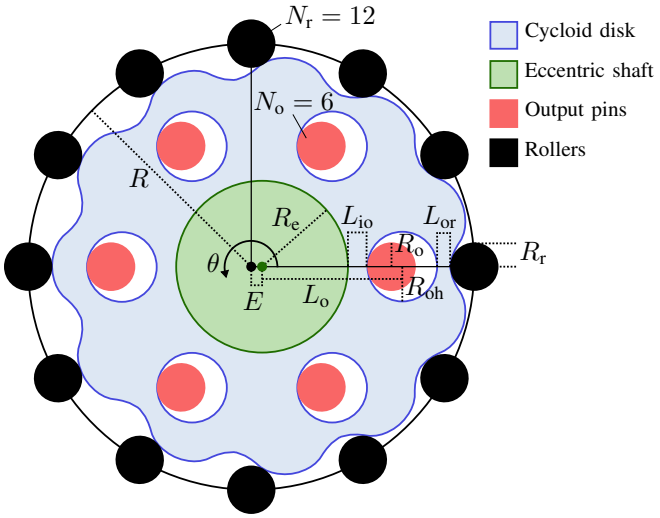

Fig. 2: Cycloidal drive geometry for a single disk.

A. Transmission ratio and cycloid disk formulation

The general expression for the reduction ratio n of a cycloidal disk with N_l lobes and N_r rollers is given by

$$n = \frac{N_\mathrm{l}}{N_\mathrm{r} - N_\mathrm{l}} \tag{1}$$

However, a difference of $N_\mathrm{r} - N_\mathrm{l} = 1$ ensures contact area for power transmission is maximised [17]. Hence, substituting $N_\mathrm{l} = N_\mathrm{r} - 1$, (1) reduces to

$$n = N_\mathrm{r} - 1 \tag{2}$$

The cycloidal disk profile may be neatly expressed by the following equations [17]:

$$\begin{aligned} c_x(\theta) &= R\cos(\theta) - R_r\cos(\theta+\psi) - E\cos(N_r\,\theta), \\ c_y(\theta) &= -R\sin(\theta) + R_r\sin(\theta+\psi) + E\sin(N_r\,\theta), \end{aligned} \tag{3}$$

where ψ denotes the angle between cycloid lobe and roller:

$$\psi = \tan^{-1}\left[\frac{\sin((N_r-1)\,\theta)}{\cos((N_r-1)\,\theta) - \frac{R}{E\,N_r}}\right], \tag{4}$$

and $\theta \in [0, 2\pi]$ denotes the angle around the input shaft.

III. Design of a 3D printed cycoidal drive

A. Requirements

The functional requirements for the cycloidal drive were set to be able to statically hold 3 kg at 1 m, with output speeds able to match most mammals [26], while remaining compact and light weight. This results in a torque capacity of ∼30 Nm and output speed of ≥25 rad/s at 48 V. A maximum mass (excl. motor) of 400 g was desired. Furthermore, we aimed for a reduction ratio of ∼10x, to maximise interaction performance and minimise output impedance (or equivalently maximise transparency), i.e. a so-called quasi-direct-drive actuator. Note that in this work we focus on the gearbox design, but combine it with a low-cost brushless motor to demonstrate its potential.

B. Design considerations

In the following we present the selection of design parameters for the 3D printed cycloidal drive. The main considerations particular to this design are the following:

FDM 3D printing: The use of Fused Deposition Modelling (FDM) 3D printing, allows for rapid manufacture of relatively complex parts at low cost. As discussed before, the large gearing contact area and absence of shear stress in cycloidal drives makes them ideally suited for 3D printing. However, care needs to be taken with regards to its limitations. Key considerations which need to be accounted for in the mechanical design are: relatively low strength of PLA, manufacturing tolerances, anisotropic properties, and minimum wall thickness and feature size. Finally, part orientation is crucial for optimal strength and accurate tolerances.

Double cycloid disks and roller bearings: Due to its mechanics, the single disk geometry shown in Fig. 2 produces an in-plane movement of the cycloidal disk's centre-of-mass. This can produce significant vibrations at high speeds. A well-known solution is to employ two disks, with 180 degree phase difference, which eliminates this problem and also halves linear forces on the components for a given torque[1]. Furthermore, to maximise efficiency, we employ miniature roller bearings for the outer rollers and output pins. Although this was already proposed in [9], it is impractical for high-ratio designs due to space constraints. [15] used needle roller bearings to ensure large contact area allowing high torque and efficiency in a compact design. We use

[1]Alternatively, a counterweight can be used for balancing. We choose a double disk design to increase torque capacity.

standard, compact, low-cost ball bearings, which combined with a low gear ratio still yields a very compact design.

Off-the-shelf components: In order to minimise cost of the design, it is advisible to use standard, off-the-shelf components. This is particularly important for selection of the roller and output pin bearings, the dimensions of which affect the entire design. Furthermore, we employ off-the-shelf steel parts (screws, nuts, and washers) for some highly loaded structural components. Note that the clearance fit of the shoulder screws and bearings allows to use nominal values for the cycloid disk profile. However, manufacturing tolerances of the used FDM printer have to be considered.

C. Design parameter selection

Selection of the design parameters starts with parameters that directly result from functional requirements (Sec. III-A). Next, dependent geometric parameters are chosen, influenced by selected components (particularly bearings). The design procedure is as follows (Fig. 2):

1) **Functional requirements:** Given required torque capacity, choose motor model and reduction ratio n. When designing for physical interaction, high-torque motors with low reduction ratio are advisible as the reflected inertia scales with n^2. When using two cycloidal disks, the number of rollers needs to be even, hence n uneven (Eq. (2)). This determines the number of rollers N_r.
2) **Bearings:** Choose small roller and output pin bearings. Their outer radius b_r defines the roller radius $R_\mathrm{r} = b_\mathrm{r}$ and output pin radius $R_\mathrm{o} = b_\mathrm{r}$. Needle bearings may be used for compactness although they can generally not be constrained in axial direction without additional friction.
3) **Outer dimensions:** Choose outer radius R. For compactness, the minimum radius is given by intersection between the rollers and undercutting constraints [18], and minimum wall thickness of the disk. We opted for the outer radius of the motor (to match housing dimensions).
4) **Cycloid disk geometry:** Choose the eccentricity E. Notice that increasing eccentricity increases the relative 'depth' of the cycloidal disk lobes, increasing its translational motion and potentially reducing the minimum wall thickness of the disk. Secondly, it increases the output hole size, weakening the disk. Third, the gearbox reflected inertia partially scales with E^2 [16]. Conversely, small eccentricty makes the cycloidal disks more circular, increasing potential for play and reduced stiffness. We found that choosing E relative to R_r provides an intuitive trade-off: For example, in our design we opted for $E = 0.45\,R_\mathrm{r}$. This parameter determines the radius of the output holes as $R_\mathrm{oh} = R_\mathrm{o} + E$.
5) **Input shaft:** Choose a larger bearing for the eccentric cam of the input shaft. Its outer radius b_e determines the shaft radius $R_\mathrm{e} = b_\mathrm{e}$. Hence, the bearing should be chosen such that 1) the shaft is constructable, and 2) sufficient space remains for the output holes: $b_\mathrm{e} < R - E - R_\mathrm{r} - R_\mathrm{oh}$.
6) **Output holes:** Lastly, given their now known size R_oh, the number of output holes N_o and their radial location L_o can be chosen, while avoiding intersection with the eccentric cam or the edge of the disk, and ensuring minimum wall thickness. These constraints are given by $L_\mathrm{io} = L_\mathrm{o} - R_\mathrm{oh} - R_\mathrm{e} \geq 0$ and $L_\mathrm{or} = R - R_\mathrm{o} - L_\mathrm{o} - R_\mathrm{oh} \geq 0$, respectively (Fig. 2). This leads to $R_\mathrm{e} + R_\mathrm{oh} < L_\mathrm{o} < R - R_\mathrm{r} - R_\mathrm{oh}$. Notice that more output pins, placed further away, reduce the linear forces per hole and pin [16].

The Python code that accompanies this paper [27] provides a straightforward way to set these parameters, reporting critical wall thicknesses and intersections.

IV. Proposed design and prototype

A. Design parameters

The geometric and functional parameters of our final design are given in Table I. The Bill-Of-Materials (BOM) for the gearbox itself is given in Table II, with total gearbox cost of only €98. Further materials and tools, including the chosen motor and electronics, are listed separately in Table III. These were chosen for convenience and usage across different prototypes, not optimised for cost.

The designed gearbox ratio is $n = 11$. Combined with the chosen motor this yields peak torque and speed well in excess of the requirements, and competitive with existing quasi-direct-drive actuators [4]. However, although most works do not report costs, this performance comes at likely significantly lower cost.

Geometric parameters		
R	41.5 mm	Outer radius (location of rollers)
N_r	12	Number of rollers
N_o	6	Number of output pins
R_r	4.5 mm	Roller radius (bearing)
R_o	4.5 mm	Output pin radius (bearing)
E	2.025 mm	Eccentricity
L_o	24.9 mm	Output hole midpoint location
R_oh	6.525 mm	Output hole radius
R_e	16 mm	Eccentric shaft radius

Functional and performance parameters	
11	Reduction ratio n (given by Eq. (2))
36.4 Nm	Nominal torque (at 40 A, thermally limited)
52.8 rad/s	Peak output speed (at 48 V)
2352 W/kg	Theoretical power density (torque × velocity / total mass)
372 g	Cycloidal gearbox mass (excl. motor)
809 g	Total mass (incl. motor and cooling)
23 mm	Gearbox thickness
104 mm	Gearbox diameter (excl. mounting flange)

TABLE I: Final design parameters.

B. CAD and prototype

Section and 3D CAD diagrams are shown in Fig. 3. Indicated are the input shaft (A), eccentric shaft (B), output disk (C), cycloid disks (D), roller pins (E), output pins (F), and stiffness ring (G). Fig. 3a shows an isometric section view of the gearbox. Notice the thickness of the entire gearbox is only 23 mm, with 104 mm housing diameter. This allows for a pancake-style implementation, particularly suitable for

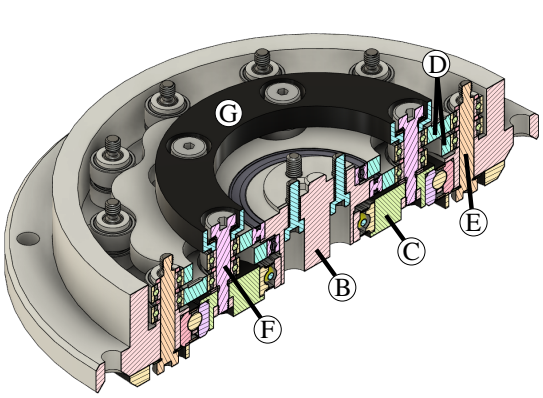

(a) Gearbox internals with lower housing removed, as seen from motor side.

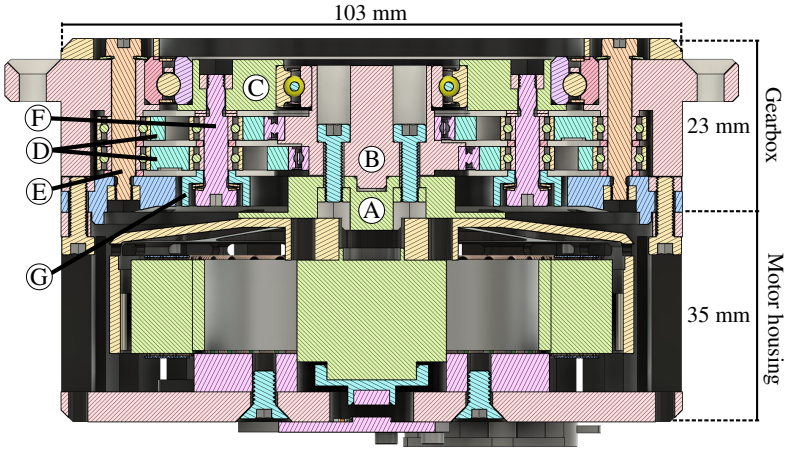

(b) Section view of full drive.

Fig. 3: CAD of the final design.

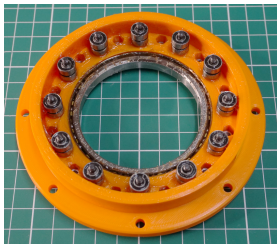

(a) Main housing.

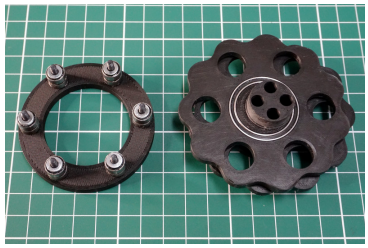

(b) Cycloidal disks and stiffness ring.

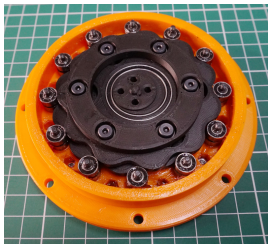

(c) Internals assembled.

(d) Assembled gearbox.

Fig. 4: Realised cycloidal gearbox prototype.

Bearings	Roller and output pin bearings (36x)	€ 15
Bearings	Eccentric shaft bearings (2x)	€ 5
Bearings	Input shaft bearing (1x)	€ 1
Bearings	Output bearing (1x)	€ 27
Screws	Shoulder screws (18x)	€ 37
Misc. steel components (screws, nuts, etc.)		€ 7
Printing	PLA filament	€ 6
	Total	**€ 98**

TABLE II: Bill-Of-Materials (BOM) of cycloidal gearbox.

Motor	T-Motor Antigravity 8012	€ 123
Motor controller	ODrive Robotics v3.6 (56 V version)	€ 179
Encoders	AMS AS5048A (2x, motor and output)	€ 32

TABLE III: Other components, materials and tools.

articulated arms or legs and exoskeletons. As mentioned previously, besides bearings, some standard steel components were used where appropriate. Specifically, a combination of embedded nuts and shoulder screws was used to accurately position the roller and output pin bearings. Assembly of housing parts uses standard M3 screws. The output disk is supported by a four-point thin section ball bearing for mechanical robustness against all types of loading.

We point out a few specific design features. First, the input shaft is double supported by a second bearing located inside of the output disk. This significantly increases its radial stiffness to forces excerted on it by the cycloid disks. Secondly, a *stiffness ring* was added, that fixes translation of the ends of the output pins with respect to each other, increasing the stiffness of the output assembly. This is similar to the so-called *subcarrier* proposed in [15].

The prototype, shown in parts in Fig. 4, was printed on a consumer-grade Prusa i3 MK3S+. Figs. 1 and 4d show the fully assembled prototype, separated from the motor. The design is fully open-source, with CAD STL/STEP files provided [27]. Furthermore, Python code to generate Fig. 2 and the animations in the video attachment are included.

V. Experimental Results

The realised prototype was validated through a series of experiments, that validate both the gearing performance as well as overall actuator performance. An experimental setup was developed (Fig. 5) that comprises a table mounting, output flange with optional pendulum, and a secondary AS5048A output encoder. All experiments were conducted with a 40 V power supply and the ODrive received commands through its Python/serial interface. Position, velocity and current data were logged via the serial interface.

A. Reduction ratio

We first validate consistency of the reduction ratio of the gearbox. Its variation affects both 1) positioning accuracy of the output based on the motor encoder, and 2) torque transmission to the output. In this experiment the drive was controlled to a constant output velocity of $\dot{q} = 2.0\,\text{rad/s}$.

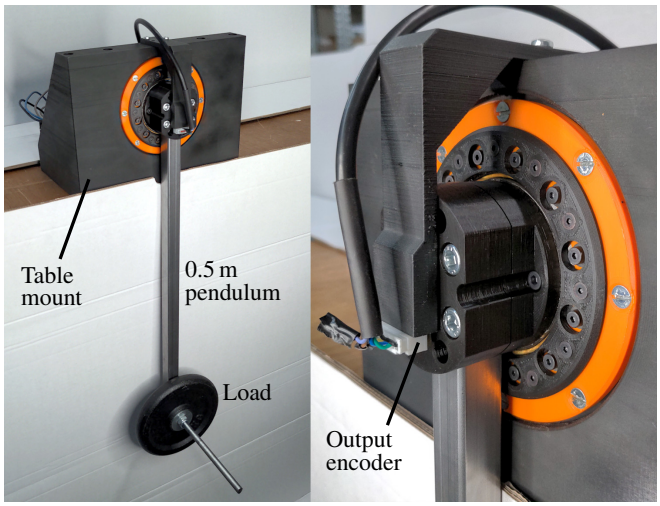

Fig. 5: Experimental setup.

Fig. 6 shows the difference between output and reduced motor angles, given by $q - \theta/n$. The data has an RMS value of 0.92 deg, or 16e−3 rad, with a maximum of 1.8 deg[2]. This corresponds to a ∼9% maximum variation in gear ratio, which is comparable to other cycloid gearing designs [13], [19]. Interestingly, a simple cosine fit of the shape

$$a_1\, cos(q + b_1) + a_2\, \cos(2\, q + b_2)$$

almost perfectly fits this data (Fig. 6), indicating that components rotating at once or twice the output speed are dominant. We speculate that tolerances between the output pins and output holes, together with inaccuracy of the output encoder position, are the main sources.

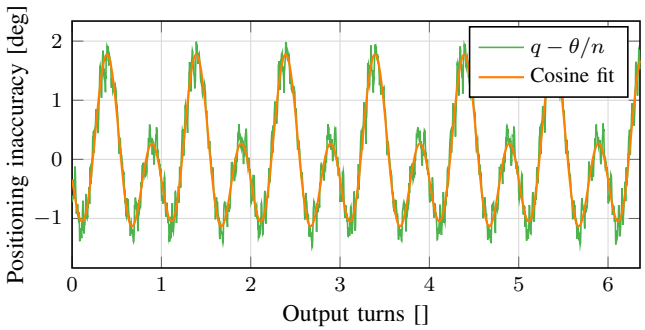

Fig. 6: Difference between output and reduced motor positions.

B. Gearing stiffness, play, and friction

Transmission stiffness was estimated by applying a series of known static loads. A heavy (∼8 kg, 0.5 m) pendulum was lifted under gravity up to 50 deg in steps of 2 deg, producing a maximum torque of 28.5 Nm. This was repeated six times, around different output positions with 60 deg increments, to account for position dependence. The resulting data is shown in Fig. 7. A linear fit produces an estimated stiffness of 633 Nm/rad.

[2]Another prototype produced 0.93 deg RMS, with 1.9 deg peak.

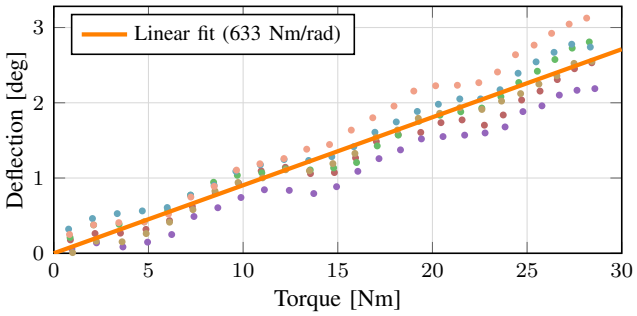

Fig. 7: Transmission stiffness.

Gearing play was estimated by comparing maximum possible output motion without resulting in motor motion, at different positions over a full output turn. Worst-case play (peak-peak) was found to be ∼0.35 deg for the prototype[3].

Transmission friction was estimated by slowly ramping between ±10 rad/s output velocity, and measuring velocity and current. Subsequently, we fit a friction model $\tau_f(\dot{q})$, comprising of Coulomb and viscous friction terms:

$$\tau_f(\dot{q}) = \begin{cases} d_c^+ + d_v^+\, \dot{q} & \text{if } \dot{q} \geq 0 \\ -d_c^- + d_v^-\, \dot{q} & \text{if } \dot{q} < 0 \end{cases}$$

Both the data and fit are shown in Fig. 8. The Coulomb friction values are ∼1% of maximum output torque. The fit yields the following friction parameters:

Coulomb [Nm]		Viscous [Nms/rad]	
d_c^+	d_c^-	d_v^+	d_v^-
0.407	0.405	0.019	0.005

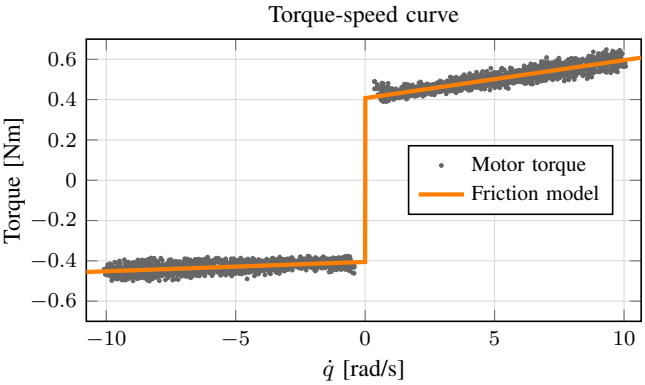

Fig. 8: Torque–speed curve and estimated friction model.

C. Position control

To test overall drive performance, we perform point-to-point position control with 1) a 380 g, 0.025 kg m^2 pendulum,

[3]Two other prototypes produced zero and 0.7 deg play, respectively. The former had slightly increased internal friction; this is a natural trade-off which may be tweaked by adjusting tolerances. Notably, a small pre-tensioning is easily achieved using plastics, without causing major changes in friction.

and 2) a 2.66 kg, 0.5 m, 0.59 kg m^2 pendulum. We utilise the ODrive's trajectory control[4], that produces continuous velocity profiles: maximum velocity and acceleration were set at 20 rad/s, 160 rad/s^2, and 10 rad/s, 10 rad/s^2, respectively.

The results are shown in Figs. 9 and 10, respectively. With the light pendulum the system is able to be very explosive, completing a half turn in 0.28 s. For the heavy pendulum, maximum acceleration was limited due to power supply limits and rigidity of the mounting apparatus. Peak speed was ∼8 rad/s. The video attachment shows these experiments, as well as impact testing and demonstrations of backdrivability.

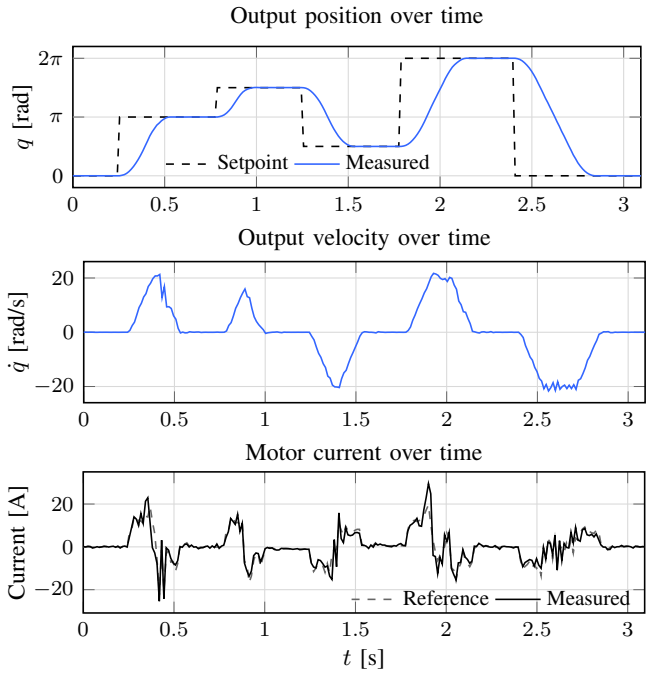

Fig. 9: Position control with 380 g, 0.025 kg m^2 pendulum: Position, velocity, and current over time.

VI. Discussion

The experimental results highlight several important points. The realised prototype demonstrated a variation in reduction ratio of ∼9%, which is comparable to existing cycloid gearing designs, but does cause positioning inaccuracy. Worst-case play and static (Coulomb) friction were small at 0.35 deg and 0.4 Nm, respectively, with very small viscous friction. These properties make the drive performant in physical interaction, which can be further improved by decogging of the motor and friction compensation. However, characterisation of the loaded efficiency curves is needed to provide further insight. The drive was tested with up to 44 Nm static loads (thermal and power supply limited) and impact/shock loading with motor accelerations of >6600 rad/s^2, without failure. Further wear, longevity, and failure testing will provide more insight, but the present prototypes have shown high robustness so far.

[4]Due to a technical limitation, data is retrieved at 100 Hz; however, control loops were executed at 8 kHz.

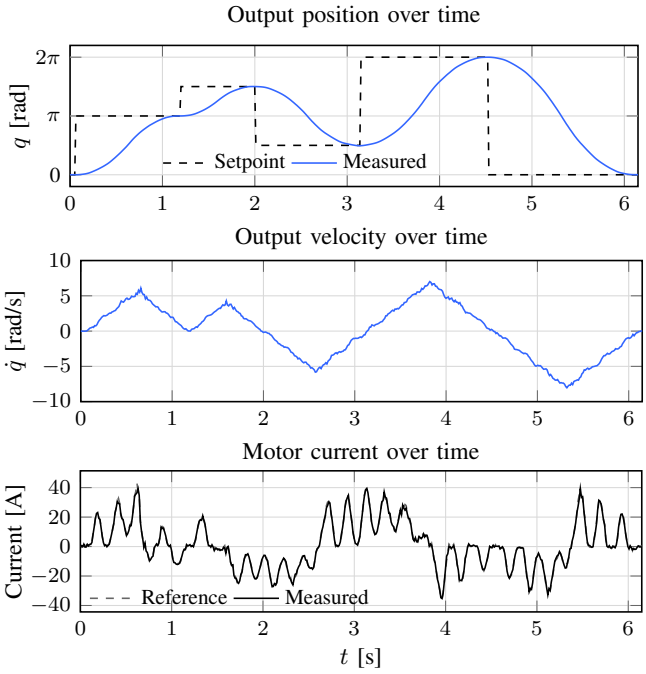

Fig. 10: Position control with 2.66 kg, 0.59 kg m^2 pendulum: Position, velocity, and current over time.

Gearing stiffness was estimated at 633 Nm/rad, which is relatively low considering the >40 Nm output torque, resulting in significant deflection at such loads. This makes accurate positioning with heavy loads difficult using only the motor encoder. We believe this aspect, and the gear ratio variation, warrant further investigation for improvement. In particular, different plastics, and embedding the output pins further into the output, could improve stiffness significantly.

VII. Conclusions & Future Work

This paper has presented a compact low-reduction cycloidal gearbox. We leverage the low cost and high availability of consumer-grade 3D printing and off-the-shelf steel components to propose a very low-cost design (€ 98) with comparatively good performance characteristics.

We have presented a parameter selection procedure that accounts for selection of the standard components, and 3D printing limitations. A prototype design was developed that was integrated with a low-cost brushless motor, creating a low-cost quasi-direct-drive. The prototype was extensively validated in experiment, showing good performance characteristics. In particular, the prototype showed low play, low friction, and high strength. This demonstrates that the chosen approach can yield a viable gearbox design. The design is fully open-source so our results can be easily replicated.

Further investigation of gear ratio variation and internal stiffness is necessary, which we recommend for future investigation. Furthermore, in-depth analysis of internal forces, friction, reflected inertia and parameter optimisation is suggested to optimally use the strengths of engineering plastics. Finally, for full quasi-direct-drive designs, low-cost frameless motors and drivers should be integrated.

REFERENCES

[1] N. Kau, A. Schultz, N. Ferrante, and P. Slade, "Stanford doggo: An open-source, quasi-direct-drive quadruped," in *2019 International Conference on Robotics and Automation (ICRA)*, May 2019. DOI: 10.1109/ICRA.2019.8794436.

[2] Y. Ding and H.-W. Park, "Design and experimental implementation of a quasi-direct-drive leg for optimized jumping," in *2017 IEEE/RSJ International Conference on Intelligent Robots and Systems (IROS)*, Sep. 2017. DOI: 10.1109/IROS.2017.8202172.

[3] F. Grimminger *et al.*, "An open torque-controlled modular robot architecture for legged locomotion research," *IEEE Robotics and Automation Letters*, vol. 5, no. 2, Apr. 2020. DOI: 10.1109/LRA.2020.2976639.

[4] A. Singh, N. Kashiri, and N. Tsagarakis, "Design of a quasi direct drive actuator for dynamic motions," in *Proceedings of 1st International Electronic Conference on Actuator Technology: Materials, Devices and Applications*, Nov. 2020. DOI: 10.3390/IeCAT2020-08516.

[5] D. V. Gealy *et al.*, "Quasi-direct drive for low-cost compliant robotic manipulation," *arXiv:1904.03815 [cs]*, Apr. 2019. arXiv: 1904.03815.

[6] P. M. Wensing *et al.*, "Proprioceptive actuator design in the MIT cheetah: Impact mitigation and high-bandwidth physical interaction for dynamic legged robots," *IEEE Transactions on Robotics*, 2017. DOI: 10.1109/TRO.2016.2640183.

[7] B. Katz, J. D. Carlo, and S. Kim, "Mini cheetah: A platform for pushing the limits of dynamic quadruped control," in *2019 International Conference on Robotics and Automation (ICRA)*, May 2019. DOI: 10.1109/ICRA.2019.8793865.

[8] S. Yu *et al.*, "Quasi-direct drive actuation for a lightweight hip exoskeleton with high backdrivability and high bandwidth," *IEEE/ASME Transactions on Mechatronics*, vol. 25, no. 4, Aug. 2020. DOI: 10.1109/TMECH.2020.2995134.

[9] J. W. Sensinger, "Efficiency of high-sensitivity gear trains, such as cycloid drives," *Journal of Mechanical Design*, vol. 135, no. 7, Jul. 2013. DOI: 10.1115/1.4024370.

[10] H. Matsuki, K. Nagano, and Y. Fujimoto, "Bilateral drive gear—a highly backdrivable reduction gearbox for robotic actuators," *IEEE/ASME Transactions on Mechatronics*, vol. 24, no. 6, pp. 2661–2673, Dec. 2019. DOI: 10.1109/TMECH.2019.2946403.

[11] S. Crispel *et al.*, "A novel wolfrom-based gearbox for robotic actuators," *IEEE/ASME Transactions on Mechatronics*, vol. 26, no. 4, pp. 1980–1988, Aug. 2021. DOI: 10.1109/TMECH.2021.3079471.

[12] P. L. García, S. Crispel, E. Saerens, T. Verstraten, and D. Lefeber, "Compact gearboxes for modern robotics: A review," *Frontiers in Robotics and AI*, vol. 7, Aug. 2020. DOI: 10.3389/frobt.2020.00103.

[13] J. W. Sensinger and J. H. Lipsey, "Cycloid vs. harmonic drives for use in high ratio, single stage robotic transmissions," in *2012 IEEE International Conference on Robotics and Automation*, May 2012. DOI: 10.1109/ICRA.2012.6224739.

[14] L. C. Farrell, J. Holley, W. Bluethmann, and M. K. O'Malley, "Cycloidal geartrain in-use efficiency study," in *Volume 5B: 42nd Mechanisms and Robotics Conference*, Aug. 2018. DOI: 10.1115/DETC2018-85275.

[15] K. Lee, S. Hong, and J.-H. Oh, "Development of a lightweight and high-efficiency compact cycloidal reducer for legged robots," *International Journal of Precision Engineering and Manufacturing*, vol. 21, no. 3, 2019. DOI: 10.1007/s12541-019-00215-9.

[16] J. W. Sensinger, "Unified approach to cycloid drive profile, stress, and efficiency optimization," *Journal of Mechanical Design*, vol. 132, no. 2, Feb. 2010. DOI: 10.1115/1.4000832.

[17] J.-H. Shin and S.-M. Kwon, "On the lobe profile design in a cycloid reducer using instant velocity center," *Mechanism and Machine Theory*, vol. 41, no. 5, May 2006. DOI: 10.1016/j.mechmachtheory.2005.08.001.

[18] Y.-W. Hwang and C.-F. Hsieh, "Geometric design using hypotrochoid and nonundercutting conditions for an internal cycloidal gear," *Journal of Mechanical Design*, vol. 129, no. 4, Apr. 2007. DOI: 10.1115/1.2437806.

[19] M Wikło, R Król, K Olejarczyk, and K Kołodziejczyk, "Output torque ripple for a cycloidal gear train," *Proceedings of the Institution of Mechanical Engineers, Part C: Journal of Mechanical Engineering Science*, vol. 233, no. 21, pp. 7270–7281, Nov. 2019. DOI: 10.1177/0954406219841656.

[20] Z.-Y. Ren, S.-M. Mao, W.-C. Guo, and Z. Guo, "Tooth modification and dynamic performance of the cycloidal drive," *Mechanical Systems and Signal Processing*, vol. 85, Feb. 2017. DOI: 10.1016/j.ymssp.2016.09.029.

[21] X. Li, C. Li, Y. Wang, B. Chen, and T. C. Lim, "Analysis of a cycloid speed reducer considering tooth profile modification and clearance-fit output mechanism," *Journal of Mechanical Design*, vol. 139, no. 3, Mar. 2017. DOI: 10.1115/1.4035541.

[22] K Olejarczyk, M Wikło, and K Kołodziejczyk, "The cycloidal gearbox efficiency for different types of bearings—sleeves vs. needle bearings," *Proceedings of the Institution of Mechanical Engineers, Part C: Journal of Mechanical Engineering Science*, vol. 233, no. 21, pp. 7401–7411, Nov. 2019. DOI: 10.1177/0954406219859903.

[23] C.-F. Hsieh, "Dynamics analysis of cycloidal speed reducers with pinwheel and nonpinwheel designs," *Journal of Mechanical Design*, vol. 136, no. 9, p. 091 008, Sep. 1, 2014. DOI: 10.1115/1.4027850.

[24] K. Wang *et al.*, "Design and control of SLIDER: An ultra-lightweight, knee-less, low-cost bipedal walking robot," in *2020 IEEE/RSJ International Conference on Intelligent Robots and Systems (IROS)*, Oct. 2020. DOI: 10.1109/IROS45743.2020.9341143.

[25] J. White, D. Swart, and C. Hubicki, "Force-based control of bipedal balancing on dynamic terrain with the "tallahassee cassie" robotic platform," in *2020 IEEE International Conference on Robotics and Automation (ICRA)*, May 2020. DOI: 10.1109/ICRA40945.2020.9196725.

[26] A. J. van Soest, A. L. Schwab, M. F. Bobbert, and G. J. van Ingen Schenau, "The influence of the biarticularity of the gastrocnemius muscle on vertical-jumping achievement," *Journal of Biomechanics*, vol. 26, no. 1, Jan. 1993. DOI: 10.1016/0021-9290(93)90608-H.

[27] W. Roozing and G. Roozing. "Cycloidal-drive." (Feb. 24, 2022), [Online]. Available: https://github.com/geez0x1/2022-cycloidal-drive.